Heavy chain-only antibodies and tetravalent bispecific antibody neutralizing *Staphylococcus aureus* leukotoxins

Benoît-Joseph Laventie[a], Hendrik Jan Rademaker[b,c], Maher Saleh[a,d], Ernie de Boer[b], Rick Janssens[b], Tristan Bourcier[a,d], Audrey Subilia[d], Luc Marcellin[d], Rien van Haperen[b,c], Joyce H. G. Lebbink[e], Tao Chen[b], Gilles Prévost[a], Frank Grosveld[b,c,f], and Dubravka Drabek[b,1]

[a]Faculté de Médecine, Physiopathologie et Médecine Translationnelle, Institut de Bactériologie, Centre Hospitalier Régional Universitaire, Université de Strasbourg, 67000 Strasbourg, France; [b]Department of Cell Biology, Erasmus Medical Center, 3000 CA Rotterdam, The Netherlands; [c]Harbour Antibodies BV, [f]Cancer Genomics Center, and [e]Departments of Genetics and Radiation Oncology, Erasmus Medical Center, 3000 CA Rotterdam, The Netherlands; and [d]Départements d'Ophtalmologie et d'Anatomie Pathologique, Centre Hospitalier Régional Universitaire, 67098 Strasbourg Cedex, France

Edited* by Richard A. Flavell, Howard Hughes Medical Institute, Yale School of Medicine, New Haven, CT, and approved August 29, 2011 (received for review February 11, 2011)

Panton–Valentine leukocidin (PVL) is a pore-forming toxin associated with current outbreaks of community-associated methicillin-resistant strains and implicated directly in the pathophysiology of *Staphylococcus aureus*-related diseases. Humanized heavy chain-only antibodies (HCAb) were generated against *S. aureus* PVL from immunized transgenic mice to neutralize toxin activity. The active form of PVL consists of the two components, LukS-PV and LukF-PV, which induce osmotic lysis following pore formation in host defense cells. One anti–LukS-PV HCAb, three anti–LukF-PV HCAbs with affinities in the nanomolar range, and one engineered tetravalent bispecific HCAb were tested in vitro and in vivo, and all prevented toxin binding and pore formation. Anti–LukS-PV HCAb also binds to γ-hemolysin C (HlgC) and inhibits HlgC/HlgB pore formation. Experiments in vivo in a toxin-induced rabbit endophthalmitis model showed that these HCAbs inhibit inflammatory reactions and tissue destruction, with the tetravalent bispecific HCAb performing best. Our findings show the therapeutic potential of HCAbs, and in particular, bispecific antibodies.

Several virulence factors, including adhesion factors and toxins, contribute to the pathology of *Staphylococcus aureus*. One of the toxins, Panton–Valentine leukocidin (PVL) is associated with human pyogenic necrotizing skin infections such as furuncles, cellulitis, and abscesses, and more severe septic infections such as osteomyelitis, bacteremia, purpura fulminans, and necrotizing pneumonia (1–8). PVL with γ-hemolysins (HlgA/HlgB and HlgC/HlgB) and LukE/LukD belongs to the bicomponent pore-forming leukotoxin family (9–14), which are thought to contribute to virulence in various infection models (15–18), although some groups disagree (19, 20). A class S and class F component interact sequentially and synergistically, inducing the activation and permeabilization of target cells and leading to their lysis. LukS-PV and LukF-PV bind to the membrane of human polymorphonuclear cells (PMNs), macrophages, and monocytes to constitute PVL (21).

Rabbit polyclonal (21) sera and polyclonal human Ig preparations (22) against PVL inhibited membrane permeabilization by the toxin in vitro, giving a rationale to use immunoglobulins in addition to antibiotics in severe staphylococcal toxemic syndrome and possibly necrotizing pneumonia. Passive immunization may have negative effects on the innate immune response at early stages of infection (23), but has very substantial advantages, including low toxicity, high specificity, and immediate effect compared with vaccines and antibiotics at late stages of infection. Immunoglobulins could be administered several times without the risk of counterimmunization, provided the antibody is human or humanized. However, to be effective, such protective toxin-neutralizing antibodies would have to be produced in sufficient quantities. HCAb, originally described in camelids (24), have no light chains and may bind epitopes unreachable by conventional antibodies (25). Consequently, HCAbs are attractive therapeutics, but would have to be humanized. Here, we evaluate the effect of one humanized anti–LukS-PV and three anti–LukF-PV HCAbs derived following antigen challenge of transgenic mice containing llama/human heavy chain Ig loci (26). Furthermore, we demonstrate that an engineered tetravalent bispecific antibody comprising both anti–LukS-PV and anti–LukF-PV humanized VH binding domains retains the functionalities of the parent HCAbs.

Results

Isolation and Characterization of Single-Domain Antibodies (sdAbs) Against LukS-PV and LukF-PV and Production of Full-Length HCAbs. Transgenic mice containing a llama/human hybrid Ig heavy chain locus (26) were immunized with recombinant LukS-PV and LukF-PV proteins. Using phage display, sdAb libraries were made from immunized animals. Three rounds of selection yielded several different positive clones. Variable heavy chain region 1 (VHH1) was used to produce HCAb against LukS-PV, whereas VHH2 was used for HCAbs against LukF-PV (Fig. 1*A*), suggesting antigen-driven VHH use. The LukS-PV VHH domains have the same 16 amino acid complementary-determining region 3 (CDR3) loop, indicating they most likely are derived from the same recombination event and therefore probably recognize the same epitope. The domains have different somatic hypermutations, and 2G12 has switched from IgG2 to IgG3. All sdAbs against LukF-PV are IgG3. Their CDR3 is shorter (11 aa) and different. There are 5.4% and 3.9% mutations per germline VHH depending on antigen used, which is comparable to that observed in the XenoMouse (27). The prediction of "humanness" or nonimmunogenicity of the obtained VHHs was evaluated by H- and G-scores (28). The llama VHH1 and VHH2 germline sequences present in the transgenic mouse have H scores of 0.753 and 0.737, respectively, and both have the best G score for human IGHV3-66 sequence (0.314 and 0.292, respectively). The HCAbs have H-scores ranging from –0.068 to 0.663, and best H-scores from –0.174 to 0.263 (*SI Appendix*, Table S1). High-affinity binders were selected by reducing the amount of antigen during selection, and those that occurred at higher frequency and low immunogenicity score were selected for further experiments.

One anti–LukS-PV (3A11) and three different anti–LukF-PV sdAbs (clones 4, 82, and 125) were subcloned into a eukaryotic expression vector containing a human IgG2 or IgG3 constant region lacking CH1 exon (*SI Appendix*) and stably transfected into human embryonic kidney (HEK) cells. Due to the presence of human VH3.23 leader sequence, the full-length HCAbs was

Author contributions: G.P., F.G., and D.D. designed research; B.-J.L., H.J.R., M.S., E.d.B., R.J., R.v.H., T.C., and D.D. performed research; T.B., J.H.G.L., and D.D. contributed new reagents/analytic tools; B.-J.L., H.J.R., A.S., L.M., G.P., F.G., and D.D. analyzed data; and G.P., F.G., and D.D. wrote the paper.

The authors declare no conflict of interest.

*This Direct Submission article had a prearranged editor.

[1]To whom correspondence should be addressed. E-mail: d.drabek@erasmusmc.nl.

This article contains supporting information online at www.pnas.org/lookup/suppl/doi:10.1073/pnas.1102265108/-/DCSupplemental.

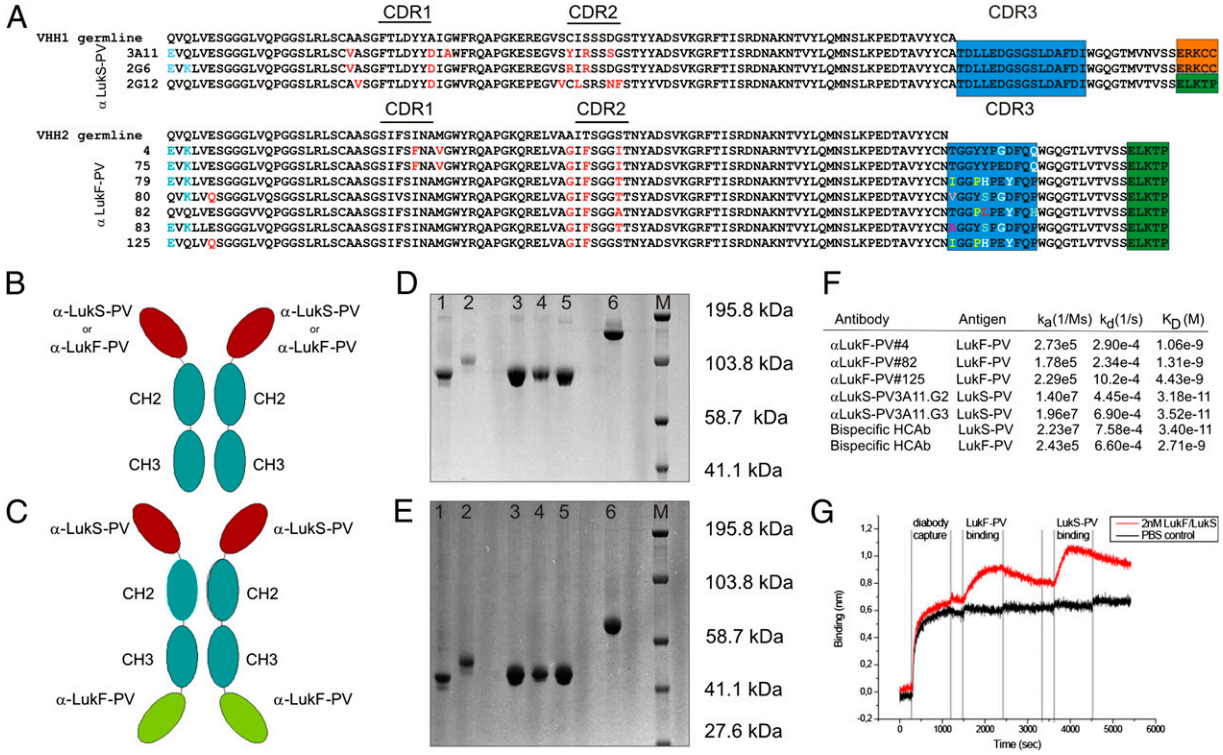

Fig. 1. (*A*) Variable region sequences of HCAbs obtained from GΔ transgenic mice after immunization with the LukS-PV and the LukF-PV proteins, showing different VHHs used for these antigens. The CDR3 loop is depicted in blue, the IgG2 hinge region in orange, and the IgG3 hinge in green blocks. Differences in the CDR3 loop are depicted in different colored letters. Somatic hypermutations are shown in red. The mutations at the 5′ end due to degenerative primer use are not counted as hypermutations. (*B*) Structural features of a full-length monospecific HCAb. (*C*) Structural features of bispecific HCAb. (*D* and *E*) HCAbs on Coomassie-stained NuPAGE 4–12% Bis-Tris gel. (*D*) Samples run under nonreduced conditions showing correct size for a dimer (85–96 kDa for monospecific HCAbs and 126 kDa for bispecific HCAb). (*E*) Samples run under reduced condition, showing correct size for the monomers (42.5–48 kDa for monospecific HCAbs and 63 kDa for bispecific HCAb). Lane 1: 3A11-G2; lane 2: 3A11-G3; lane 3: 4-G3, lane 4: 82-G3; lane 5: 125-G3; lane 6: 3A11-4-G3. (*F*) Summary of the affinity data for mono- and bispecific HCAbs. (*G*) Binding of bispecific HCAb first to LukF-PV, followed by binding to LukS-PV using Octet QK.

secreted and purified from serum-free medium using protein A agarose. All full-length HCAbs are ∼80–90 kDa dimmers, as expected for IgG2 or IgG3 (Fig. 1*D*). Under reducing conditions, all gave rise to single chains of 40–45 kDa (Fig. 1*E*).

Generation and Characterization of Bispecific Tetravalent HCAb. The highest-affinity anti–LukF-PV antibody (Fig. 1*F*) was chosen to generate a bispecific anti–LukS-PV/anti–LukF-PV tetravalent antibody (Fig. 1*C*) that binds both LukS-PV and LukF-PV antigens simultaneously. (Fig. 1*G*). The VHH of anti–LukF-PV-4 was cloned onto the C terminus of the anti–LukS-PV IgG3 without the CH1 exon. The stop codon was removed to allow translation into the anti–LukF-PV domain via a flexible synthetic linker (ERKPPVEPPPPP). The secreted antibody is a dimer of ∼120 kDa that runs as a single moiety on FPLC (Fig. 1*D* and *SI Appendix*, Fig. S2).

The half-life of the bispecific antibody was similar to a regular human antibody after in vivo injection of the antibodies in the bloodstream of mice lacking a functional heavy chain locus (μMT) (29) and measuring antibody left in the serum at different times after injection (*SI Appendix*, Fig. S3 *A* and *B*). The functional stability assay performed by incubating the antibody with human serum shows that at day 18, the anti–LukS-PV3A11G3 and anti-SF bispecific antibody retain 80% and 63% inhibitory pore forming activity, respectively, and 90% and 82% of their capacity to inhibit LukS-PV binding to hPMNs membranes at day 0 (*SI Appendix*, Fig. S3 *C* and *D*).

Binding Affinity and Specificity of HCAbs. Affinity measurements showed the 3A11-G2 and 3A11-G3 HCAbs to be in the same range regardless of constant region (K_d ∼3×10^{-11} M; Fig.1*F*). The K_d for anti–LukF-PV antibodies 4, 82, and 125 are of nanomolar range: 1.06×10^{-9} M, 1.31×10^{-9} M, and 4.43×10^{-9} M, respectively (Fig. 1*F*). The affinity of bispecific full-length antibody for each individual antigen is the same for LukS-PV, but slightly reduced for LukF-PV; importantly, this antibody binds both antigens simultaneously (Fig. 1*G* and *SI Appendix*, Fig. S4).

HCAbs against LukS-PV do not recognize LukF-PV; conversely, HCAbs against LukF-PV do not detect LukS-PV (*SI Appendix*, Fig. S1), which excludes the possibility that the antibodies recognize common epitopes present in both recombinant proteins. The bispecific HCAb obviously detects both LukS-PV and LukF-PV (*SI Appendix*, Figs. S1 and S4 and Fig. 1*G*). Further analysis showed that other bicomponent leukotoxins (HlgA/HlgB, HlgC/HlgB, and LukE/LukD) are not inhibited, except anti–LukS-PV HCAb also inhibiting the γ-hemolysin couple HlgC/HlgB (*SI Appendix*, Fig. S5). The inhibitory activity of the HCAbs was, therefore, also tested against HlgC/HlgB leukotoxin.

Assessment of HCAb Inhibitory Function in Vitro. Leukotoxins exert their action by (*i*) binding of S and F proteins to target cell membranes (21, 30); (*ii*) oligomerization and rapidly increasing intracellular calcium concentrations independently of pore formation and cell activation (12, 31); and (*iii*) reconfiguration of S and F proteins to form functional pores permeable to monovalent cations (32). The capacity of antibodies to inhibit these three steps was tested.

Inhibition of pore formation was investigated first. Increasing concentrations of any HCAbs delayed the start of ethidium entry and gave a decrease of the entry slope. As the PVL control reached its maximum about 40 min after toxin addition, we calculated the IC_{50} of ethidium entry. The IC_{50} for anti–LukS-PV 3A11 and the bispecific antibody were 1.14 nM and 0.31 nM, respectively, against PVL (LukS-PV 0.1 nM/LukF-PV 5 nM; Fig. 2*A*) and 0.10

and 0.12 nM, respectively, against HlgC/HlgB (HlgC 0.1 nM/HlgB 0.5 nM; Fig. 2*C*). The IC_{50} for anti–LukF-PV 4, 82, 125, and the bispecific antibody 3A11-4 were 0.93, 0.91, 0.65, and 1.44 nM, respectively, against PVL (LukS-PV 1 nM/LukF-PV 1 nM; Fig. 2*B*). Complete PVL inhibition was reached >3 nM of anti–LukS-PV and 0.3 nM for γ-hemolysin. This inhibition is stable in time (maximum tested: 2 h). Complete PVL inhibition was reached >7 nM of anti–LukF-PV. If a higher amount of anti–LukS-PV 3A11 or anti–LukF-PV 4 (7 nM) is added 5 or 15 min after toxin addition to hPMNs, it stabilizes but does not reduce the ethidium entry slope (*SI Appendix*, Fig. S6 *A* and *B*). Thus, the antibodies block neo-pore formation, but not already formed pores.

Human PMNs are activated by very low concentration of leukotoxins, and, thus, activation is difficult to avoid. Calcium entry in hPMNs relies on leukotoxins compounds binding and oligomerization (33). We measured variation of intracellular calcium concentrations in hPMNs by flow cytometry. Log IC_{50} were calculated as the percentage of control calcium entry slope (*SI Appendix*, Table S2). IC_{50} for anti–LukS-PV 3A11 and the diabody 3A11-4 were 1.12 and 0.79 nM, respectively, against PVL, and 0.41 and 0.44 nM, respectively, against HlgC/HlgB (Fig. 2 *D* and *F*). A complete PVL and HlgC/HlgB inhibition was reached >10 nM antibody. The three anti–LukF-PV 4, 82, 125, and the diabody 3A11-4 gave IC_{50} of 7.07, 9.33, and 8.71 nM, respectively (Fig. 2*E*). Complete PVL inhibition was reached above 30 nM of anti–LukF-PV HCAbs in our conditions.

The binding of labeled leukotoxin proteins (LukS-PV*, LukF-PV*, and HlgB*) to hPMNs membranes was followed using flow cytometry. Increased concentrations of the anti–LukS-PV 3A11 and the bispecific anti-PVL 3A11-4 decreases LukS-PV* binding, and for both antibodies binding IC_{50}s are ≤10 nM for concentrations of LukS-PV* up to 10 nM (Fig. 2*G*). The inhibition profile is similar for these two antibodies. Increasing concentrations of any of the three anti–LukF-PV 4, 82, and 125 HCAbs decreased the amount of LukF-PV* fluorescence on hPMNs membranes. The inhibition power of the three anti–LukF-PV HCAbs was comparable (*SI Ap-*

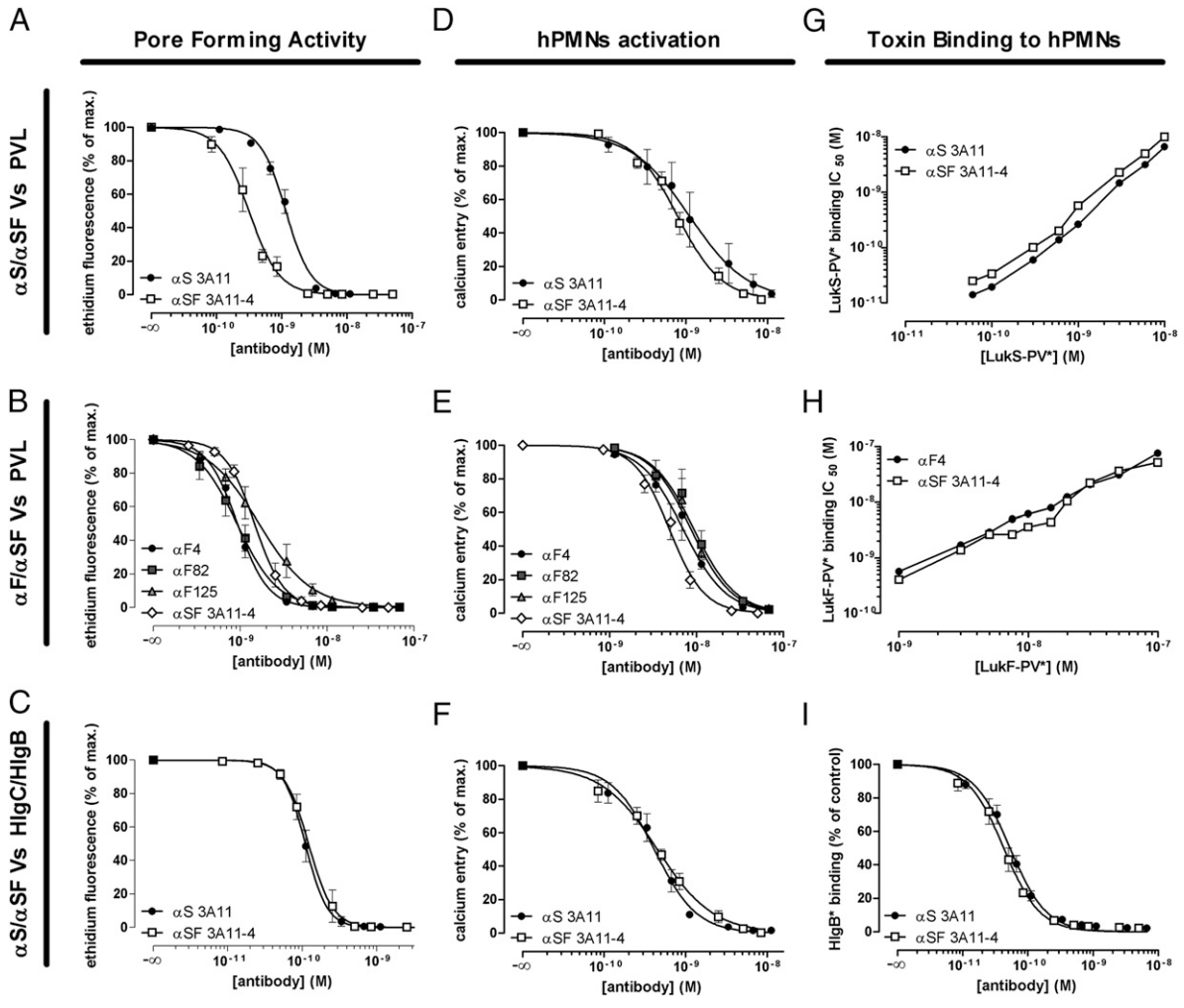

Fig. 2. The inhibitory capacities of antibodies against pore formation, hPMNs activation, and leukotoxins components binding. For PVL (*A*, *B*, *D*, and *E*), limiting concentrations of LukS-PV were used for assays with anti–LukS-PV, or LukF-PV, for assays with anti–LukF-PV. (*C*, *F*, and *J*) HlgC/HlgB inhibition. Pore formation and hPMNs activation inhibition: ethidium or calcium entry into hPMNs induced by PVL (LukS-PV 0.1 nM/LukF-PV 5 nM: *A* and *D*; LukS-PV 1 nM/LukF-PV 1 nM: *B* and *E*) or HlgC/HlgB (HlgC 0.1 nM/HlgB 0.5 nM: *C* and *F*) in the presence of various concentrations (10^{-10} nM to 10^{-7} nM) of αS 3A11, αF 4, αF 82, αF 125, or αSF 3A11-4. Reported values are ethidium fluorescence at $t = 40$ min or calcium entry slopes. PVL components binding inhibition: LukS-PV* (*G*) or LukF-PV* (*H*) in combination with various concentration of αS 3A11, αF 4, or αSF 3A11-4 were added to hPMNs suspensions at $t = 0$ and recorded at equilibrium as cell-associated fluorescein fluorescence. IC_{50} were calculated. Data are expressed as binding IC_{50} (M) for each combination of concentrations. A similar experiment was conducted to inhibit HlgB* fluorescence, which reflects HlgC binding onto hPMNs membranes, at toxin concentration 0.1 nM HlgC/0.5 nM HlgB* (*I*). Reported values represent the percentage of maximum control HlgB* fluorescence without antibody. Error bars represent SEM for at least three independent experiments counting 3,000 events each time.

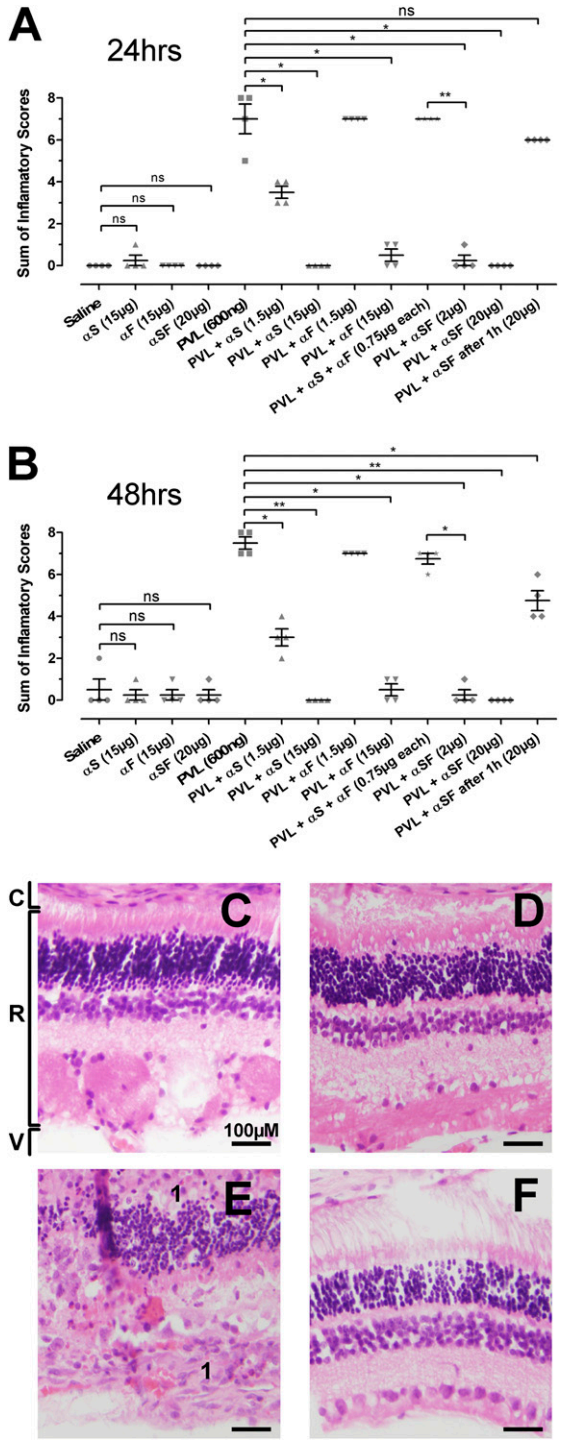

Fig. 3. Effect of HCAbs in a rabbit model of toxin-induced endophthalmitis after 24 h (*A*) and 48 h (*B*) postinjection. The inflammatory scores (*Materials and Methods*) were measured after injections of 50 μL of physiological saline solution containing PVL (600 ng) and/or HCAb (0.75, 1.5, or 15 μg of anti–LukS-PV 3A11 and/or anti–LukS-PV 4, 2, or 20 μg of diabody 3A11-4) into the vitreous of rabbit eyes. Higher inflammatory scores represent a higher level of inflammation, with increasing damages and lesions of the anterior and posterior chamber of the eye. Error bars represent SEM. (*C–F*) Optic microscopy of H&E-stained rabbit retina slides of an eye 48 h after intravitreal injection of PBS (*C*), 15 μg anti–LukS-PV 3A11 antibody (*D*), 600 ng PVL (*E*), or 600 ng PVL + 15 μg anti–LukS-PV 3A11 (*F*). Accolades: C, choroid; R, retina; V, vitreous. Note that retinal detachment is artifactual. Despite low anatomic variation of retina layers thickness, injection of either PBS or antibody preserves the retinal organization. Injection of 600 ng PVL disrupts retinal architecture, and "1" indicates massive lymphocyte infiltrate. Injection of PVL + antibody shows a preservation of retinal architecture, very similar to that of the normal eye.

pendix, Fig. S7). LukF-PV* binding inhibition was extensively studied for anti–LukF-PV 4 and for the bispecific anti-PVL 3A11-4 with various LukF-PV* concentrations, and for both antibodies, binding IC_{50} are ≤10 nM for concentrations of LukF-PV* up to 25 nM (Fig. 2*H*). Addition of anti–LukS-PV 3A11 or anti-PVL 3A11-4 also decreased HlgC/HlgB* binding (Fig. 2*I*), by acting on HlgC binding.

The binding IC_{50} was also very low on monocytes and lymphocytes (*SI Appendix*, Fig. S8). We conclude that the antibodies specifically recognize targeted PVL proteins, preventing PVL proteins binding to hPMNs, monocytes, and lymphocytes.

Neutralizing Effect of HCAbs in Vivo. The effectiveness of anti-PVL HCAbs in inhibiting PVL-associated diseases was tested in a non-infectious model of rabbit intravitreous PVL injection. The clinical and histological observations in one group of rabbits of a given injection were similar. A healthy untreated eye was also included to control for histopathology. It shows that the retinal detachment is artifactual. Injection of PBS was used as a control, because both toxins and antibodies were diluted in PBS. Double-blind readings for the control show a reaction level of 0 in anterior and posterior chambers 24 and 48 h after injection (Fig. 3 *A* and *B*). After 48 h, histological analysis showed an absence of inflammatory infiltrate or vascular congestion in iris, conjunctiva, and retina, and a minimal vascular congestion of the choroid (Fig. 3*C*). The injection of an antibody only (15 μg of anti–LukS-PV or anti–LukF-PV or 20 μg of diabody) induced almost no reaction with a mean inflammatory score below 0.5 for anterior and 0 for posterior chambers, with a minimal vascular congestion of iris and choroid, and a minimal retinal inflammatory deposit, with preservation of the overall retina organization (Fig. 3*D*). PVL injection (300 ng LukS-PV + 300 ng LukF-PV) induces a high inflammatory response (score 3 or 4) in the anterior chamber, hiding the posterior chamber (assumed score 4). Intense vascular congestion of the iris and an intense inflammatory infiltrate of the choroid was seen, whereas the retina has lost its architecture and was replaced by a purulent lysis (Fig. 3*E*). Injection of PVL together with 1.5 μg of anti–LukS-PV or anti–LukF-PV or 2 μg of diabody (each represents 10 nM of antibody assuming a volume of a rabbit eye of 1.5 mL) was sufficient to significantly reduce the inflammatory score at 24 h postinjection from 7 to 3.5 (1.5–2 for each chamber) for anti–LukS-PV ($P = 0.024$, one-tailed) and to 0.3 for the diabody ($P = 0.012$, one-tailed), whereas no effect was seen with this dose of anti–LukF-PV (Fig. 3*A*). Injections of 15 μg of anti–LukS-PV or anti–LukF-PV or 20 μg of the diabody rendered PVL totally inefficient to produce damage, as measured by a significantly reduced global inflammatory score <0.5 (Fig. 3*A*; $P < 0.014$, one-tailed). These scores remain the same at 48 h postinjection (Fig. 3*B*). The histological analysis shows a small inflammatory infiltrate of the iris, none or minimal vascular congestion of the iris and choroid, and minimal inflammatory infiltrate in retina, whose overall architecture is preserved for the example of 15 μg of anti–LukS-PV (Fig. 3*F*). Importantly, injection of 0.75 μg anti–LukS-PV together with 0.75 μg anti–LukF-PV did not significantly reduce the inflammatory score, whereas the same molar amount of diabody (2 μg) totally prevented such inflammation (Fig. 3 *A* and *B*), and we conclude that the same molar amount of tetravalent antibody dimer is more effective than the bivalent HCAb dimers. Rabbits were followed for 4, 7, and 14 d after injections of antibodies. The rabbits never showed any difficulties in moving or eating, and reactivity and vision appeared to be efficient. When 20 μg of the diabody was injected 1 h after injection of PVL (600 ng), a significantly decreased inflammatory response was observed at 48 h for the sum of the two scores (score = 4.75, $P < 0.05$, one-tailed; Fig. 3*B*), and the score continued to increase between 24 and 48 h without antibody. Such a result is in agreement with pre-

vious observations that antibodies cannot neutralize already formed pores, but are effective in preventing new pore formation.

Discussion

We show that specific high-affinity HCAb can be derived from transgenic mice. The specificity and binding affinity is maintained in the tetravalent bispecific antibodies. Importantly, both the bivalent HCAb and the tetravalent HCAb are stable in vivo. The anti-PVL antibodies have demonstrated their ability to inhibit the binding step of their target protein in a weak molar excess; they can interfere in vitro both with soluble proteins and with already bound proteins, provided they are not engaged into a pore. The anti–LukS-PV 3A11 HCAb also inhibits pore formation on target cells by a HlgB/HlgC γ-hemolysin pair. Because HlgB is unable to bind directly to hPMNs membranes, and only binds to previously bound HlgC (21), we concluded from the experiment with labeled HlgC-Cys*∼HlgB complex, that 3A11 HCAb binds HlgC, preventing its binding to the membrane. This is not surprising, because LukS-PV and HlgC have 81% protein sequence identity and most probably share the same epitope recognized by 3A11 HCAb. This result is also in agreement with the report that LukS–PV and HglC compete for the same binding site, whereas HlgA and LukE do not (34). LukS-PV and HlgC also share Trp^{275}, an amino acid residue essential for HlgC binding to monosialoganglioside on the leukocyte membrane (35). In contrast to the PVL locus, genes encoding γ-hemolysins are present in almost all clinical strains, thus 3A11HCAb could be used to block action of the HlgC/HlgB γ-hemolysin pair.

S. aureus is among the leading causes of postoperative and posttraumatic infections. For endophthalmitis, it is associated with poor visual outcome. Tissue destruction in *S. aureus* endophthalmitis results partially from combined effects of several exotoxins that contribute to severity of endophthalmitis by accelerating the rate of retinal damage onset. The toxic effect of the expression of PVL and leukotoxins has been demonstrated in rabbit eye (14), where they (including α-hemolysin) participate in inflammation and virulence (15, 36–38). Here, we show that HCAbs are also biologically active in vivo by neutralizing the PVL effect in rabbit eye vitreous. Though the inflammatory condition of eyes injected with PVL aggravate at 48 h, the inhibition achieved with antibodies is stable in time (48 to >96 h) without apparent default in vision or behavior. Though in vitro experiments performed on PMNs with antibody in high antibody excess show equal performance, in vivo data at lower excess show that the same molar amount of tetravalent antibody dimer is more effective than the bivalent HCAb dimers. Thus, the tetravalent complex has the obvious advantage that it is more effective at a lower dose and that it consists of a single chain, which is easy to produce. Our results suggest the possibility of antibody application in combination with intravitreal antimicrobial management strategy for postcataract surgery endophthalmitis and possibly other infections. Thus, these antibodies have to be tested in infection models to evaluate their potential to rapidly reduce the inflammation. More HCAbs neutralizing most *S. aureus* pore-forming toxins could be developed in the future to control toxin-related inflammatory processes in *S. aureus*-related diseases; they might limit tissue lesions and complement antimicrobial treatment.

Materials and Methods

Bacterial Expression and Production/Purification of Recombinant LukS-PV and LukF-PV Proteins Used for Immunization and in Vivo Studies. DNA coding for LukS-PV and LukF-PV was amplified from *S. aureus* Panton–Valentine positive strain isolated from patient material (generous gift from the Microbiology Department of Erasmus Medical Center) expressed in *E. coli* B21 and purified as described in *SI Appendix*.

Immunization, Phage Display Library, ELISAs, and HCAb Production. Five GΔ transgenic mice containing hybrid llama/human Ig loci (26) were immunized with 20 μg of recombinant LukS-PV or LukF-PV protein five times in 2-wk intervals. The immunization protocol, phage display library, ELISAs, and antibody production after transfection in HEK cells were performed as described in *SI Appendix*.

In Vitro Affinity Measurements. Kinetics of antibody/antigen interactions were determined using Biacore T100 (GE Healthcare). A CM5 sensor chip (GE Healthcare) was coated with anti-human IgG using the amino-coupling procedure as described by the manufacturer. Antibodies (∼10 fmol) were captured onto this surface using PBS with 0.01% Tween 20 at 25 °C. Antigen (LukF-PV 0.4–13 nM; LukS-PV 0.25–4.0 nM) were flowed over the chip at 30 μL/min. Association and dissociation rate constants were determined by fitting a 1:1 binding model to the data using the Biacore T100 Evaluation Software version 2.0.1. The binding of bispecific HCAb was also assessed on the Octet QK (ForteBio Inc.; *SI Appendix*).

PMNs Purification. Human PMNs from healthy donors were purified from buffy coats as previously reported (13) and suspended at 5×10^5 cells/mL in 10 mM Hepes, 140 mM NaCl, 5 mM KCl, 10 mM glucose, 0.1 mM EGTA (pH 7.3).

Flow Cytometry Measurements. Flow cytometry measurements from 3,000 PMNs were carried out using a FACSort flow cytometer (Becton-Dickinson) equipped with a 15-mW argon laser tuned to 488 nm. Pore formation was assessed by the penetration of ethidium bromide (EtBr) through the pores. We evaluated the intracellular calcium entry in cells (5×10^5 cells/mL) previously loaded with 5 μM Fluo-3 (Molecular Probes) in the presence of 1.1 mM extracellular Ca^{2+} by measuring the increase of Fluo-3 fluorescence. Cells were incubated for 10 min with 4 μM EtBr before the addition of toxins in the absence of extracellular calcium. EtBr or Fluo-3 fluorescence was measured from the fluorescence light 3 (λ_{Em} = 650 nm) and 1 (λ_{Em} = 530 nm) using Cell Quest Pro software (Becton-Dickinson). To evaluate the inhibition capacity of antibodies, PVL (0.1 nM LukS-PV + 5 nM LukF-PV when using anti–LukS-PV HCAb; 1 nM each when using anti–LukF-PV HCAb), γ-hemolysin (HlgA 2nM; HlgB 0.5 nM, HlgC 0.1 nM), or LukE/LukD (2 nM or 20 nM respectively) were preincubated for 10 min with increasing concentrations of antibodies (0–10 μg/mL), together with 4 μM EtBr, in the absence of extracellular calcium to follow EtBr entry, or in the presence of 1.1 mM $CaCl_2$ to follow calcium entry in PMNs. Concurrently, PMNs (5×10^5 cells/mL) were preincubated for 10 min with 4 μM EtBr bromide, or for 5 min with 1.1 mM $CaCl_2$, and the flow cytometric measurements were started immediately after addition of the leukotoxin/antibody mixture. The results from at least three different healthy donors were averaged and expressed as percentages of a control: ethidium fluorescence of dead cells or calcium entry slope of the toxin without antibodies. Baseline values were obtained for each series of data from a control without addition of toxin, and were systematically subtracted from the other assays.

Leukotoxins Binding Assays. Binding assays were carried out with fluorescein-labeled LukS-PV G10C* at 0.06/0.1/0.3/0.6/1/3/6/10 nM, Cys*∼LukF-PV at 1/3/5/7.5/10/15/20/30/50/100 nM, Cys*∼HlgA at 2 nM, and Cys*∼HlgB at 0.5 nM under the same conditions as nonlabeled proteins. The amount of labeled protein bound on the cell surface is measured by flow cytometry as the cell fluorescence from FL1 (5×10^5 cells/mL).

Data Analysis. Data analysis was performed using GraphPad Prism version 5.04 for Windows (GraphPad Software). Log IC_{50} and log IC_{50} SEM were given by GraphPad Prism using a nonlinear regression dose–response inhibition equation.

Antibody Stability Assay in Human Serum. Antibodies (5 μM) were incubated in decomplemented human serum lacking anti-PVL activity for 0, 1, 3, 6, 9, 12, and 18 d at 37 °C. Pore formation and labeled LukS-PV* binding to hPMNs were recorded for each time point by flow cytometry as previously described, and IC_{50} were calculated using PRISM software.

Rabbits and Eye Injections. All experimental procedures were conducted in accordance with the Association for Research in Vision and Ophthalmology Statement for the Use of Animals in Ophthalmic and Vision Research and the permission (no. A67-482-8) given by the French Ministry of Forests and Agriculture. Injections were performed as described in Siqueira et al. (14). Inoculums of 50 μL of physiological saline solution containing PVL (600 ng) and/or HCAb (1.5 or 15 μg) or tetravalent bispecific HCAb (2 or 20 μg) were injected into eyes through the *pars plana* into the vitreous with a 25-gauge needle, avoiding the crystalline lens and retina and slowly removing the needle to prevent a backward flow of toxin under the conjunctiva.

Clinical Investigations. Direct ophthalmoscopy was performed 24 h and 48 h after vitreous injections. Observed vitreal inflammatory activity of the posterior chamber was graded according to criteria given by Nussenblatt et al. (39). Briefly, five increasing levels of severity of damage were defined: 0, normal eye without vitreous haze; 1, vitreous haze allowing ob-

servation of the optic nerve and retinal vessels; 2, vitreous haze still allowing observation of vessels and optic nerve, but with difficulty; 3, vitreous haze allowing observation of the optic nerve only, its boundaries being blurred; and 4, vitreous haze preventing observation of the optic nerve. We also used standardized criteria that grade severity of damage to the anterior chamber and its annexes (14) in five levels: 0, normal eye with no physical damage; 1, a slight conjunctival hyperaemia located around the site of injection; 2, the presence of conjunctival hyperaemia involving at least half of the surface and associated with a scant discharge, but without haze in the anterior chamber; 3, moderate secretion, slight blepharitis, total conjuctival hyperaemia, perikeratic injection, chemosis, and slight haze of the anterior chamber, still allowing observation of iris; and 4, total conjuctival hyperaemia, blepharitis and edema, chemosis, and secretion with significant haze of the anterior chamber preventing the observation of iris. The "global inflammatory score" represents the sum of two grades obtained for each eye segment separately. In cases where more eyes/rabbits were injected, we calculated the average inflammatory score for a given injection.

Histopathological Analysis. Anesthetized rabbits were euthanized 48 h after the experimental intravitreous injection and clinical examination, by i.v. injection of 5 mL pentobarbital commercial solution (= 1 g Dolethal; Vétoquinol). Eyeballs were cautiously enucleated to avoid retinal detachment, intravitreously injected through the optic nerve with 500 μL of 4% wt/vol paraformaldehyde in 0.1 M phosphate buffer (pH 7.2), and fixed for >24 h by immersion in the same 4% wt/vol paraformaldehyde solution and 24 h in alcohol. After being embedded in paraffin, 4-μm slides were prepared, dewaxed, and H&E stained (Cover-Tech CTM6; Microm) before microscopy (BX60 microscope; Olympus). Pictures were taken using a DP70 Digital Microscope Camera (Olympus).

Statistical Analysis. A bilateral nonparametric Mann–Whitney *U* test was used for comparative analysis of inflammatory scores of eyes injected with saline and eyes injected with antibodies only. A unilateral nonparametric Mann–Whitney *U* test was used for comparative analysis of inflammatory scores of eyes injected with PVL and eyes injected with PVL + antibody. Statistical analysis was performed using GraphPad Prism version 5.04 for Windows (GraphPad Software).

ACKNOWLEDGMENTS. We thank Raymonde Girardot and Daniel Keller for technical assistance, Dr. C. Moog for cells, and Roger Craig and Geoff Davis for helpful comments. B.-J.L. was supported by a PhD grant from the Ministère de l'Enseignement Supérieur et de la Recherche. Support was also provided by Direction de la Recherche et des Etudes Supérieures Grant EA-4438, the Cancer Genomics Center, the Netherlands Organization for Scientific Research, and Harbour Antibodies BV.

1. Adler A, Temper V, Block CS, Abramson N, Moses AE (2006) Panton-Valentine leukocidin-producing *Staphylococcus aureus*. *Emerg Infect Dis* 12:1789–1790.
2. Durupt F, et al. (2007) Prevalence of *Staphylococcus aureus* toxins and nasal carriage in furuncles and impetigo. *Br J Dermatol* 157:1161–1167.
3. Holmes A, et al. (2005) *Staphylococcus aureus* isolates carrying Panton-Valentine leucocidin genes in England and Wales: Frequency, characterization, and association with clinical disease. *J Clin Microbiol* 43:2384–2390.
4. Kravitz GR, Dries DJ, Peterson ML, Schlievert PM (2005) Purpura fulminans due to *Staphylococcus aureus*. *Clin Infect Dis* 40:941–947.
5. Laporte-Turpin E, et al. (2006) Necrotizing pneumonia and arthritis due to *Staphylococcus aureus* producing Panton and Valentine leukocidin in a 10-year-old boy. *Arch Pediatr* 13:449–452.
6. Mitchell PD, Hunt DM, Lyall H, Nolan M, Tudor-Williams G (2007) Panton-Valentine leukocidin-secreting *Staphylococcus aureus* causing severe musculoskeletal sepsis in children. A new threat. *J Bone Joint Surg Br* 89:1239–1242.
7. Yamasaki O, et al. (2005) The association between *Staphylococcus aureus* strains carrying Panton-Valentine leukocidin genes and the development of deep-seated follicular infection. *Clin Infect Dis* 40:381–385.
8. Gillet Y, et al. (2002) Association between *Staphylococcus aureus* strains carrying gene for Panton-Valentine leukocidin and highly lethal necrotising pneumonia in young immunocompetent patients. *Lancet* 359:753–759.
9. Gravet A, et al. (2001) *Staphylococcus aureus* isolated in cases of impetigo produces both epidermolysin A or B and LukE-LukD in 78% of 131 retrospective and prospective cases. *J Clin Microbiol* 39:4349–4356.
10. Prévost G, et al. (1995) Panton-Valentine leucocidin and gamma-hemolysin from *Staphylococcus aureus* ATCC 49775 are encoded by distinct genetic loci and have different biological activities. *Infect Immun* 63:4121–4129.
11. Sugawara N, Tomita T, Sato T, Kamio Y (1999) Assembly of *Staphylococcus aureus* leukocidin into a pore-forming ring-shaped oligomer on human polymorphonuclear leukocytes and rabbit erythrocytes. *Biosci Biotechnol Biochem* 63:884–891.
12. Baba Moussa L, et al. (1999) Discoupling the Ca(2+)-activation from the pore-forming function of the bi-component Panton-Valentine leucocidin in human PMNs. *FEBS Lett* 461:280–286.
13. Gravet A, et al. (1998) Characterization of a novel structural member, LukE-LukD, of the bi-component staphylococcal leucotoxins family. *FEBS Lett* 436:202–208.
14. Siqueira JA, et al. (1997) Channel-forming leucotoxins from *Staphylococcus aureus* cause severe inflammatory reactions in a rabbit eye model. *J Med Microbiol* 46:486–494.
15. Bronner S, et al. (2003) Moxifloxacin efficacy and vitreous penetration in a rabbit model of *Staphylococcus aureus* endophthalmitis and effect on gene expression of leucotoxins and virulence regulator factors. *Antimicrob Agents Chemother* 47:1621–1629.
16. Diep BA, et al. (2010) Polymorphonuclear leukocytes mediate *Staphylococcus aureus* Panton-Valentine leukocidin-induced lung inflammation and injury. *Proc Natl Acad Sci USA* 107:5587–5592.
17. Diep BA, et al. (2008) Contribution of Panton-Valentine leukocidin in community-associated methicillin-resistant *Staphylococcus aureus* pathogenesis. *PLoS ONE* 3:e3198.
18. Labandeira-Rey M, et al. (2007) *Staphylococcus aureus* Panton-Valentine leukocidin causes necrotizing pneumonia. *Science* 315:1130–1133.
19. Olsen RJ, et al. (2010) Lack of a major role of *Staphylococcus aureus* Panton-Valentine leukocidin in lower respiratory tract infection in nonhuman primates. *Am J Pathol* 176:1346–1354.
20. Voyich JM, et al. (2006) Is Panton-Valentine leukocidin the major virulence determinant in community-associated methicillin-resistant *Staphylococcus aureus* disease? *J Infect Dis* 194:1761–1770.
21. Meyer F, Girardot R, Piémont Y, Prévost G, Colin DA (2009) Analysis of the specificity of Panton-Valentine leucocidin and gamma-hemolysin F component binding. *Infect Immun* 77:266–273.
22. Gauduchon V, et al. (2004) Neutralization of *Staphylococcus aureus* Panton Valentine leukocidin by intravenous immunoglobulin in vitro. *J Infect Dis* 189:346–353.
23. Yoong P, Pier GB (2010) Antibody-mediated enhancement of community-acquired methicillin-resistant *Staphylococcus aureus* infection. *Proc Natl Acad Sci USA* 107: 2241–2246.
24. Hamers-Casterman C, et al. (1993) Naturally occurring antibodies devoid of light chains. *Nature* 363:446–448.
25. Lauwereys M, et al. (1998) Potent enzyme inhibitors derived from dromedary heavy-chain antibodies. *EMBO J* 17:3512–3520.
26. Janssens R, et al. (2006) Generation of heavy-chain-only antibodies in mice. *Proc Natl Acad Sci USA* 103:15130–15135.
27. Mendez MJ, et al. (1997) Functional transplant of megabase human immunoglobulin loci recapitulates human antibody response in mice. *Nat Genet* 15:146–156.
28. Thullier P, Huish O, Pelat T, Martin AC (2010) The humanness of macaque antibody sequences. *J Mol Biol* 396:1439–1450.
29. Kitamura D, Roes J, Kühn R, Rajewsky K (1991) A B cell-deficient mouse by targeted disruption of the membrane exon of the immunoglobulin mu chain gene. *Nature* 350:423–426.
30. Gauduchon V, Werner S, Prévost G, Monteil H, Colin DA (2001) Flow cytometric determination of Panton-Valentine leucocidin S component binding. *Infect Immun* 69: 2390–2395.
31. Nguyen VT, Higuchi H, Kamio Y (2002) Controlling pore assembly of staphylococcal gamma-haemolysin by low temperature and by disulphide bond formation in double-cysteine LukF mutants. *Mol Microbiol* 45:1485–1498.
32. Comai M, et al. (2002) Protein engineering modulates the transport properties and ion selectivity of the pores formed by staphylococcal gamma-haemolysins in lipid membranes. *Mol Microbiol* 44:1251–1267.
33. Staali L, Monteil H, Colin DA (1998) The staphylococcal pore-forming leukotoxins open Ca2+ channels in the membrane of human polymorphonuclear neutrophils. *J Membr Biol* 162:209–216.
34. Menestrina G, et al. (2003) Ion channels and bacterial infection: The case of beta-barrel pore-forming protein toxins of *Staphylococcus aureus*. *FEBS Lett* 552:54–60.
35. Nishiyama A, Kaneko J, Harata M, Kamio Y (2006) Assembly of staphylococcal leukocidin into a pore-forming oligomer on detergent-resistant membrane microdomains, lipid rafts, in human polymorphonuclear leukocytes. *Biosci Biotechnol Biochem* 70:1300–1307.
36. Bronner S, Stoessel P, Gravet A, Monteil H, Prévost G (2000) Variable expressions of *Staphylococcus aureus* bicomponent leucotoxins semiquantified by competitive reverse transcription-PCR. *Appl Environ Microbiol* 66:3931–3938.
37. Dajcs JJ, Thibodeaux BA, Girgis DO, O'Callaghan RJ (2002) Corneal virulence of *Staphylococcus aureus* in an experimental model of keratitis. *DNA Cell Biol* 21:375–382.
38. Girgis DO, et al. (2005) Pathogenesis of Staphylococcus in the rabbit anterior chamber. *Invest Ophthalmol Vis Sci* 46:1371–1378.
39. Nussenblatt RB, Palestine AG, Chan CC, Roberge F (1985) Standardization of vitreal inflammatory activity in intermediate and posterior uveitis. *Ophthalmology* 92:467–471.